Bifunctional Bioorganometallic Iridium(III)–Platinum(II) Complexes Incorporating Both Intercalative and Covalent DNA Binding Capabilities

Susan Gençaslan[a] and William S. Sheldrick*[a]

Keywords: Iridium / Platinum / Peptides / DNA binding / Bioinorganic chemistry

The DNA binding of bifunctional Ir^{III}–Pt^{II} complexes containing $[(\eta^5\text{-Cp}^*)Ir(dppz)]^{2+}$ and $[Pt(terpy)]^{2+}$ or *trans*-$[PtL_2L']^{2+}$ fragments (L = NH_3, L′ = DMF; L = H_2O, L′ = NH_3) bridged by flexible κ*S*:κ*N*(amino)-coordinated methionine-containing peptides has been studied by UV/Vis and CD spectroscopy. Stable intercalative binding of the Ir^{III} fragment of the complexes $[\{(\eta^5\text{-Cp}^*)Ir(dppz)\}(\mu\text{-peptide-}\kappa S{:}\kappa N)\{Pt(terpy)\}](CF_3SO_3)_4$ (**5**) (peptide = H-Gly-Gly-Phe-Met-OH; H-Gly-OH = glycine, H-Phe-OH = L-phenylalanine, H-Met-OH = L-methionine) and **6** [peptide = H-$(Ala)_4$-Met-OH; H-Ala-OH = L-alanine] is indicated by their steady decrease in absorbance at maxima between 350 and 390 nm on titration with CT DNA and by the bathochromic shifts of these maxima. Binding constants K_b of $1.4(4)\times10^6$ M^{-1} for both **5** and **6** and site sizes *s* of 2.8(1) and 2.2(1), respectively, are in accordance with this monofunctional mode. Both peptide chain length and the site(s) of the labile Pt^{II} substituents DMF or H_2O play an important role in determining the degree of intercalation of the Ir^{III} fragment and the extent of helix distortion caused by simultaneous covalent binding of Pt^{II} centres for the DNA interaction of the complexes $[\{(\eta^5\text{-Cp}^*)Ir(dppz)\}(\mu\text{-peptide-}\kappa S{:}\kappa N)\{trans\text{-}(PtL_2L')\}]^{4+}$ **7**–**10**. Whereas both **9** and **10** (L = H_2O, L′ = NH_3; peptide = H-Gly-Met-OH or H-Gly-Gly-Met-OH) exhibit a high degree of bifunctional binding [**9**, K_b = $1.1(5)\times10^6$ M^{-1}, *s* = 1.3(1); **10**, K_b = $1.4(7)\times10^6$ M^{-1}, *s* = 2.1(1)], CD spectroscopy indicates that a more pronounced reorganisation of the DNA helix is required for the former complex with its shorter peptide. Effective intercalation is also observed for **8** (L = NH_3, L′ = DMF; peptide = H-Gly-Gly-Met-OH) but not for **7** with the analogous Pt^{II} fragment but a shorter bridging peptide (H-Gly-Met-OH).

Introduction

Multinuclear platinum complexes containing two or more square-planar platinum(II) centres capable of covalent binding to DNA nucleobases represent a relatively new class of anticancer agents.[1–3] They have been shown to exhibit activity in cancer cell lines with intrinsic resistance to cisplatin and can also overcome acquired resistance to this successful antitumor drug, presumably as a result of their participation in long-range interstrand DNA adducts. Length, conformational flexibility, total charge and hydrogen-bonding donor capacity of the linking ligands (e.g. 1, *n*-diaminoalkanes) have been identified by Farrell[1,2] as paramount factors in the design of multinuclear platinum drugs.

A modified approach to the polynuclear concept involves the design of bifunctional complexes with two distinct DNA binding capabilities connected by a rigid or flexible bridging moiety. For instance octahedral ruthenium(II) and square-planar platinum(II) centres have been linked in the heterodinuclear complexes $[\{cis\text{-}RuCl_2(Me_2SO)_3\}(\mu\text{-}H_2N(CH_2)_4NH_2)\{cis\text{-}PtCl_2(NH_3)\}]$[4] and [(terpy)Ru(μ-dtdeg)PtCl]Cl_3 {terpy = 2,2′:6′,2′′-terpyridine, dtdeg = bis[4′-(2,2′:6′,2′′-terpyridyl)]diethyleneglycol ether}.[5] However, the light-sensitive and highly reactive former complex proved to be unsuitable as a DNA binding probe and the latter complex exhibited a lower cytotoxicity towards cisplatin-sensitive cell lines in comparison to $[PtCl(terpy)]\cdot2H_2O$, presumably due to the fact that its ruthenium moiety can only participate in electrostatic DNA interactions. Attempts to improve on the effectiveness of cisplatin have also involved the tethering of intercalating acridine[6,7] and phenazine[8,9] groups to platinum(II) centres. The presence of an intercalative chromophore leads both to a marked increase in the rate of DNA platination and to an altered sequence specificity.[7,9] Metallointercalators such as $[Pt(terpy)]^{2+}$[10,11] or $[Ru(dppz)(phen)_2]^{2+}$ (dppz = dipyrido[3,2-*a*:2′,3′-*c*]phenazine)[12] have also been linked to identical fragments to afford bifunctional complexes with high DNA binding affinities. The use of dppz-containing compounds to promote intercalative DNA binding is well documented.[13]

We have recently demonstrated that bioorganometallic metallointercalators of the type $[(\eta^5\text{-Cp*})Ir(dppz)(peptide)]^{n+}$ (*n* = 1–3)[14] and $[(\eta^6\text{-arene})Ru(dppz)(peptide)]^{n+}$ (*n* = 1–3; arene = C_6H_6, $Me_3C_6H_3$, C_6Me_6)[15] exhibit strong side-on intercalative binding into DNA with equilibration constants K_b of up to 5.5×10^6 M^{-1}. Following initial

[a] Lehrstuhl für Analytische Chemie, Ruhr-Universität Bochum, 44780 Bochum, Germany
Fax: +49-234-32-14742
E-Mail: William.Sheldrick@ruhr-uni-bochum.de

chemospecific κ*S* coordination of the organometallic [(η^5-Cp*)Ir(dppz)]$^{2+}$ or [(η^6-arene)Ru(dppz)]$^{2+}$ fragment in complexes of methionine-containing peptides, a second similar or different metal fragment can be introduced by employing either the terminal amino function or the donor atom of a suitable side chain as the additional binding site. The feasibility of this concept has been demonstrated for [{(η^5-Cp*)Ir(dppz)}$_2$(μ-H-Met-Met-OH-κ*S*:κ*S*′)](CF$_3$SO$_3$)$_4$ and [{(η^5-Cp*)Ir(dppz)}(μ-H-Gly-Met-OH-κ*S*:κ*N*$_G$){Pt(terpy)}](CF$_3$SO$_3$)$_4$.[16] We now extend the design strategy to iridium(III)–platinum(II) complexes exhibiting an intercalating [(η^5-Cp*)Ir(dppz)]$^{2+}$ moiety tethered to a *trans*-[PtL$_2$L′] (L = NH$_3$, H$_2$O;L′ = DMF, NH$_3$) fragment. To the best of our knowledge, such compounds of the type [{(η^5-Cp*)Ir(dppz)}(μ-peptide-κ*S*:κ*N*){*trans*-(PtL$_2$L′)}]$^{4+}$ represent the first examples of bifunctional complexes containing both a metallointercalator and a covalent DNA binding capability.

Results and Discussion

Monofunctional Starting Compounds [(η^5-Cp*)Ir(dppz)(peptide-κ*S*)](CF$_3$SO$_3$)$_2$ 3 and 4

The bioorganometallic starting compounds of the type [(η^5-Cp*)Ir(dppz)(peptide-κ*S*)](CF$_3$SO$_3$)$_2$ [peptide = H-Gly-Met-OH,[16] H-Gly-Gly-Met-OH,[14] H-Gly-Gly-Phe-Met-OH (**3**), H-(Ala)$_4$-Met-OH (**4**)] were prepared as described previously for H-Gly-Met-OH[16] and H-Gly-Gly-Met-OH[14] by initially refluxing [(η^5-Cp*)Ir(acetone)$_3$](CF$_3$SO$_3$)$_2$ (**1**)[17] with dppz in CH$_3$OH/CH$_2$Cl$_2$ for 2 h. Addition of the appropriate peptide in CF$_3$COOH to the resulting [(η^5-Cp*)Ir(acetone)(dppz)](CF$_3$SO$_3$)$_2$ solution leads to formation of the desired complexes [(η^5-Cp*)-Ir(dppz)(peptide-κ*S*)](CF$_3$SO$_3$)$_2$ (Scheme 1). Strongly acidic conditions (CF$_3$COOH) are, however, necessary to achieve chemospecific κ*S* coordination of the methionine side chains in the presence of non-protected terminal amino or carboxylate groups. After stirring at 50 °C for 18 h and volume reduction, the products can be precipitated by addition of diethyl ether. The remaining solution contains a residual quantity of [(η^5-Cp*)Ir(CF$_3$COO)(dppz)](CF$_3$SO$_3$) (**2**), which could be subsequently crystallised in low yield.

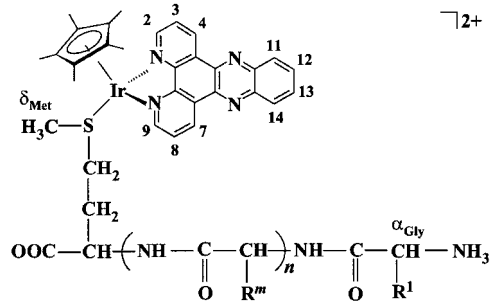

3 $R^3 = CH_2\text{-}C_6H_5$, $R^2 = R^1 = H$ ($n = 2$; $m = 2, 3$)
4 $R^1 - R^4 = CH_3$ ($n = 3$; $m = 2, 3, 4$)

Scheme 1.

As depicted in Figure 1, complex **2** exhibits an interplanar angle of 56.1° between its Cp* and dppz ring systems and contains a κ*O*-coordinated trifluoroacetate ligand with an Ir–O2 distance of 2.156(7) Å. Although individual [(η^5-Cp*)Ir(CF$_3$COO)(dppz)]$^+$ cations dimerise through π–π interactions of their parallel phenanzine ligands in the crystal structure of **2** (Figure 2), more extensive base stacking is prevented by the steric requirements of the Cp* and CF$_3$COO$^-$ ligands. An interplanar distance of 3.48 Å is observed for the dppz ring systems within such cation pairs. Dimerisation of complexes containing the [(η^5-Cp*)-Ir(dppz)]$^{2+}$ fragment will, of course, be expected in solution and also possibly as an external binding mode on the DNA surface for the bifunctional complexes studied in the present work. This prompted us to determine the dimerisation constant K_D for [(η^5-Cp*)Ir(dppz)(H-Gly-Gly-Met-OH-κ*S*)](CF$_3$SO$_3$)$_2$ as a typical monofunctional member of this class of bioorganometallic compounds.

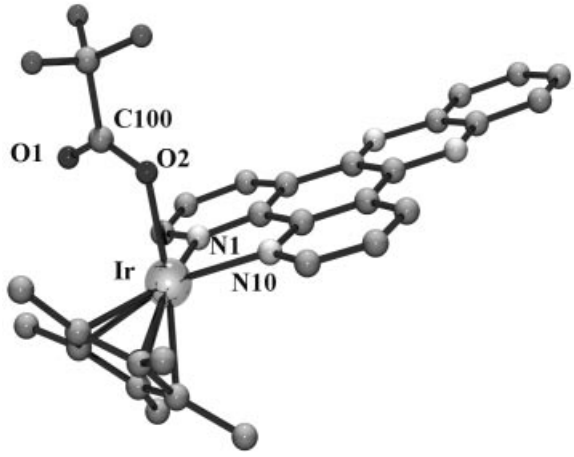

Figure 1. Molecular structure of the cation of [(η^5-Cp*)-Ir(CF$_3$COO)(dppz)](CF$_3$SO$_3$) (**2**): Selected bond lengths [Å] and angles [°]: Ir–N1 2.109(8), Ir–N10 2.106(8), Ir–O2 2.156(7), Ir–C 2.158(4)–2.198(4), C100–O1 1.20(2), C100–O2 1.26(1), N1–Ir–N10 77.4(3), N1–Ir–O2 84.6(3), N10–Ir–O2 82.9(3).

The [(η^5-Cp*)Ir(dppz)(H-Gly-Gly-Met-OH)]$^{2+}$ cation displays two characteristic absorption maxima at 364 and 382 nm for the π–π* transitions of its dppz ligand. At very low concentrations (10 μM or lower) in a 10 mM phosphate buffer at pH = 7.2, the molar absorption coefficients ε_{364} and ε_{382} are independent of the cation concentration, i.e. **2** is present as a monomer. The observed hypochromic shifts in the ε values for the concentration range 10–180 μM (Figure 3) are indicative of increasing intermolecular dipole–dipole interactions between dppz ligands and thereby of dimerisation. Using the equation of Schwarz et al.,[18] a dimerisation constant K_D of 6.4×10^3 M^{-1} was determined on the basis of a regression analysis for ($\varepsilon_M - \varepsilon_{obsd.}$) ($\lambda$ = 382 nm) in the concentration range 10–250 μM. Respective values of 13395 L·mol^{-1}·cm^{-1} and 8894 L·mol^{-1}·cm^{-1} were obtained for the molar absorption constants ε_M and ε_D of the monomer and dimer. These represent a relative decrease in absorption $\Delta A/A$ at 382 nm of 25.4%. The strength of the base stacking for the large planar dppz ligands of [(η^5-Cp*)Ir(dppz)(H-Gly-Gly-Met-OH)]$^{2+}$ is underlined by

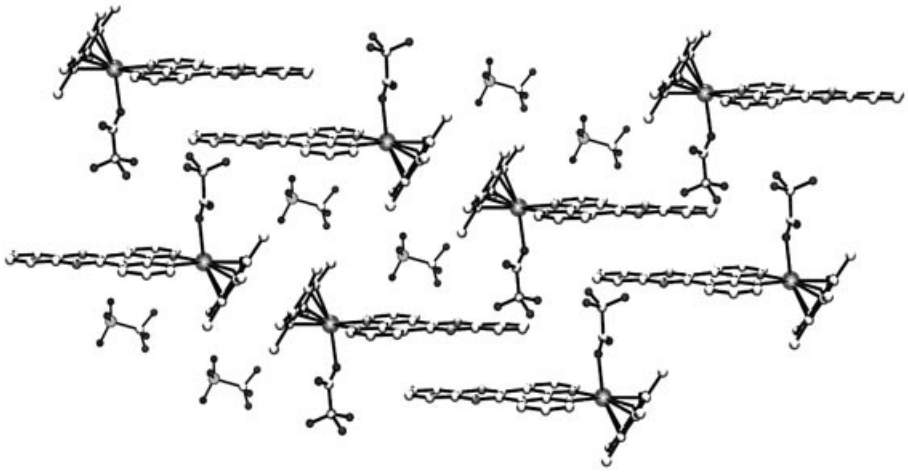

Figure 2. Dimerisation of the $[(\eta^5\text{-Cp*})Ir(CF_3COO)(dppz)]^+$ cations of **2** in the crystal lattice.

comparing its K_D value with the lower values of 4×10^3 and 5×10^2 M^{-1} for [PtCl(terpy)]Cl[19] and proflavine.[18]

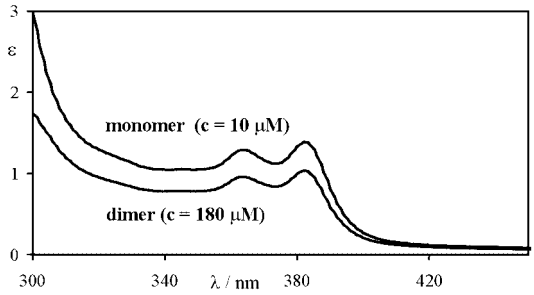

Figure 3. Dimerisation of the $[(\eta^5\text{-Cp*})Ir(dppz)(H\text{-}Gly\text{-}Gly\text{-}Met\text{-}OH)]^{2+}$ cations in a phosphate buffer at pH = 7.2 as demonstrated by the hypochromic shift of the molar absorption coefficients ε ($L \cdot mol^{-1} \cdot cm^{-1}$) in the wavelength range 300–420 nm.

Bifunctional Iridium(III)–Platinum(II) Metallointercalators 5 and 6

The bifunctional iridium(III)–platinum(II) metallointercalators $[\{(\eta^5\text{-Cp*})Ir(dppz)\}(\mu\text{-H-Gly-Gly-Phe-Met-OH-}\kappa S{:}\kappa N_G)\{Pt(terpy)\}](CF_3SO_3)_4$ (**5**) and $[\{(\eta^5\text{-Cp*})Ir(dppz)\}(\mu\text{-H-(Ala)}_4\text{-Met-OH-}\kappa S{:}\kappa N_G)\{Pt(terpy)\}](CF_3SO_3)_4$ (**6**) (Figure 4) are prepared by addition of **3** or **4**, respectively, to an aqueous $[Pt(OH_2)(terpy)](CF_3SO_3)_2$ solution. All four complexes were characterised by elemental analysis, FAB mass spectrometry, ^{1}H and ^{13}C NMR, IR and UV/Vis spectroscopy. Downfield ^{1}H NMR shifts of 0.10 ppm are observed for the signals of the Cp* methyl protons of the κ*S*-coordinated $[(\eta^5\text{-Cp*})Ir(dppz)]^{2+}$ fragments in **3**–**6** in comparison to the δ value of 1.74 for this singlet in a CD_3OD solution of the chloro complex $[(\eta^5\text{-Cp*})Ir(Cl)(dppz)](CF_3SO_3)$.[14] In contrast, the signals of the methionine δ-CH_3 protons adjacent to the coordinated thioether sulfur atoms in the met-containing complexes exhibit a more pronounced opposite upfield shift from typical values of ca. 2.10 ppm in the free peptide to resonance positions in the range δ = 1.79–1.81 ppm. As previously noted for both $[(\eta^5\text{-Cp*})Ir(dppz)]^{2+}$ and $[(\eta^6\text{-arene})Ru(dppz)]^{2+}$ derivatives[14,15] this behaviour represents a striking reversal of the typical positive shift displayed by the signals of the δ-CH_3 protons in analogous half-sandwich organometallic complexes without a chelating aromatic ligand such as dppz.[20,21] The shielding cone of the neighbouring dppz ligand may well be responsible for this anomalous upfield shift in **3**–**6**.

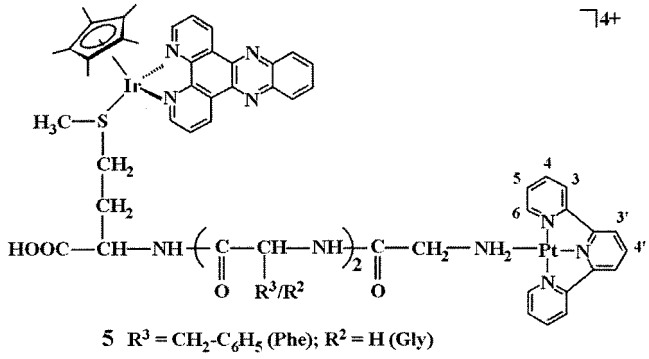

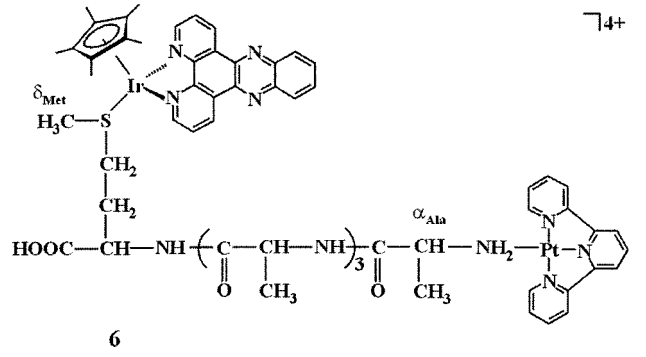

Figure 4. Tetracations of the bifunctional complexes **5** and **6**.

Additional κ*N* coordination of the $[Pt(terpy)]^{2+}$ fragment by the terminal amino group of the peptide ligands in **5** and **6** leads to significant upfield shifts in the δ values of the H6

and H5 protons from their resonance positions of δ = 9.00 and 7.86 ppm in [PtCl(terpy)]Cl (CD_3OD solution). Respective shifts of δ = 8.83/8.88 and 7.82 ppm are observed for the bifunctional complexes. Further clear evidence for κ*N* coordination is also provided by the characteristic upfield shifts recorded for the signals of the adjacent α proton(s) of the terminal amino acid residue in **5** and **6**. Whereas the α_{Gly1} singlet exhibits only a modest shift from δ = 3.65 ppm in the free peptide to 3.61 ppm upon coordination in **5**, a striking move from δ = 3.94 to 3.72 ppm is observed for signal of the α_{Ala1} proton in **6**.

DNA Binding Studies for 3–6

A pronounced decrease in absorbance at 364 and 382 nm and the bathochromic shifts of these absorption maxima (Figure 5) on UV/Vis titration of 20 μM solution of **3**–**6** with calf thymus DNA (CT DNA) are clearly indicative of dppz intercalation into DNA. In contrast to the hypochromic shifts $-\Delta A/A$ of 32.1–38.7% for **3**–**6** at 382 nm with their associated red shifts of 5 nm, a much smaller decrease in absorbance of only 12.2 or 11.0%, respectively, is observed for the terpyridine ligand at its 343 nm maximum in **5** and **6**, which remains unshifted. As no correction for the increase in DNA absorbance at 343 nm (due to its 15-fold increase in concentration during the UV/Vis titration) was made, it is reasonable to assume that terpyridine intercalation will not be of great significance for the binding of **5** and **6**. Absorption data collected at 382 nm for **3**–**6** were fitted by least squares using the non-cooperative non-specific binding model by Bard and Thorp.[22,23] Best fits were obtained for the intrinsic binding constants K_b and the average binding site sizes *s* listed in Table 1. Both these parameters and the melting temperature shifts ΔT_m for **3** and **4** are closely similar to the values of $1.2(1)\times10^6$ M^{-1} (K_b), 1.6 (*s*) and 6.9 °C (ΔT_m) previously reported for the analogous compound [(η^5-Cp*)Ir(dppz)(H-Gly-Gly-Met-OH-κ*S*)](CF$_3$SO$_3$)$_2$.[14] We chose the longer oligopeptides H-Gly-Gly-Phe-Met-OH and H-(Ala)$_4$-Met-OH in the hope that these might enable long-range bis-intercalation of their bifunctional complexes **5** and **6** into the DNA helix.

However, as simultaneous intercalation of both the aromatic ligands of the [(η^5-Cp*)Ir(dppz)]$^{2+}$ and [Pt(terpy)]$^{2+}$ fragments would be predicted to afford significantly higher binding constants and site sizes [i.e. the average number of nucleobase pairs between the specific or middle binding position of neighbouring mono- or bis-metallointercalators, respectively], the calculated values of 1.4×10^6 M^{-1} and 2.8(1)/2.2(1) for K_b and *s* in **5** and **6** are clearly in accordance with effectively exclusive [(η^5-Cp*)Ir(dppz)]$^{2+}$ mono-intercalation. We have previously reported similar binding constants [$1.5(1)\times10^6$ M^{-1} and $3(3)\times10^6$ M^{-1}] and site sizes (2.6, 2.9) which also indicate only mono-intercalation of the Ir^{III} fragment for two likewise intercalators [{(η^5-Cp*)-Ir(dppz)}$_2$(μ-H-Met-Met-OH-κ*S*:κ*S*′)](CF$_3$SO$_3$)$_4$ and [{(η^5-Cp*)Ir(dppz)}(μ-H-Gly-Met-OH-κ*S*:κ*N*$_G$){Pt(terpy)}]-(CF$_3$SO$_3$)$_4$.[16] These values, taken together with the successful fitting of the UV/Vis data for all complexes in a wide complex/DNA molar ratio {*r* = 0.067–1.0 with [DNA] = M(nucleotide)} indicate that the DNA binding mode of such metallointercalators must be effectively independent of the number of amino acid residues. Whereas the extended aromatic system of dppz preferentially intercalates into DNA, the stabilising role of the smaller terpyridine ligands will presumably be restricted to intermolecular base stacking on the DNA surface. The relatively limited decrease in absorbance at the terpy maximum (λ = 343 nm) observed during UV/Vis titrations is in accordance with this binding description (Figure 5). Interestingly, the highest K_b and *s* values were determined for the H-Gly-Met-OH complex, thereby suggesting that such surface π–π interactions may, indeed, be more favourable for the [Pt(terpy)]$^{2+}$ moiety when bridged to the Ir^{III} fragment by this shorter peptide.

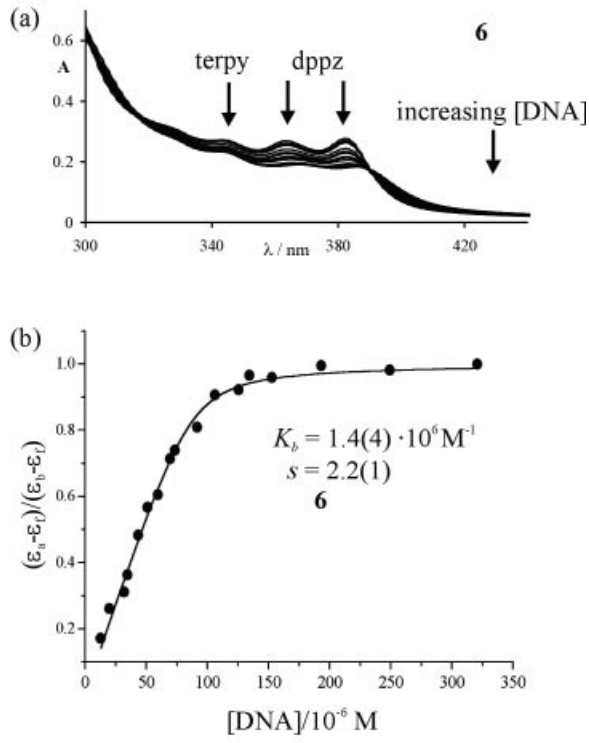

Figure 5. (a) UV/Vis spectra for the titration of [{(η^5-Cp*)Ir(dppz)}-[μ-(Ala)$_4$-Met-OH-κ*S*:κ*N*]{Pt(terpy)}](CF$_3$SO$_3$)$_4$ **6** (20 μM) in a 10 mM phosphate buffer (pH = 7.2) with CT DNA [0–300 μM (nucleotide)]; (b) the best least-squares fit for **6**/DNA to the non-cooperative non-specific binding model by Bard and Thorp.[22,23]

Table 1. Binding constants K_b, site sizes *s* and melting temperature shifts ΔT_m for the interaction of CT DNA with complexes **3**–**6** in a 10 mM phosphate buffer at pH = 7.2.

Complex	K_b [M^{-1}]	s	ΔT_m [°C]
3	$2.3(3)\times10^6$	2.6(1)	5.2
4	$1.0(3)\times10^6$	1.8(1)	5.2
5	$1.4(4)\times10^6$	2.8(1)	7.2
6	$1.4(4)\times10^6$	2.2(1)	8.2
Ref.[14][a]	$1.2(1)\times10^6$	1.6(1)	6.9

[a] For [(η^5-Cp*)Ir(dppz)(H-Gly-Gly-Met-OH-κ*S*)](CF$_3$SO$_3$)$_2$.

Bifunctional Iridium(III)–Platinum(II) Complexes 7–10 with Both Intercalative and Covalent DNA Binding Capabilities

Treatment of the appropriate monofunctional starting compound $[(\eta^5\text{-Cp*})Ir(dppz)(peptide\text{-}\kappa S)](CF_3SO_3)_2$ with *trans*-$[Pt(DMF)_2(NH_3)_2](NO_3)_2$ in DMF affords the bifunctional complexes $[\{(\eta^5\text{-Cp*})Ir(dppz)\}(\mu\text{-peptide-}\kappa S{:}\kappa N_{G1})(trans\text{-}\{Pt(NH_3)_2DMF\})](CF_3SO_3)_2(NO_3)_2$ (peptide = H-Gly-Met-OH **7**, H-Gly-Gly-Met-OH **8**) shown in Figure 6. The required *trans*-$[Pt(DMF)_2(NH_3)_2](NO_3)_2$ is prepared in situ by addition of 2 equiv. of $AgNO_3$ to *trans*-$[PtCl_2(NH_3)_2]$ in DMF solution followed by filtration of the precipitated AgCl. Retention of the κ*S* coordination mode by the $[(\eta^5\text{-Cp*})Ir(dppz)]^{2+}$ fragment is confirmed by the characteristic ^{1}H NMR upfield shifts of the methionine δ-CH_3 singlets to δ = 1.79 ppm in **7** and **8**. Replacement of the Ir^{III} fragment by *trans*-$[Pt(DMF)(NH_3)_2]$ would, in contrast, lead to a downfield shift for the signals of these protons from δ ≈ 2.10 ppm in the free peptides to a value in the range δ = 2.3–2.5 ppm.[24,25] Coordination of the Pt^{II} moiety by the N-terminal glycine (Gly1) amino function in **7** and **8** is indicated by the pronounced upfield shifts of the α_{Gly1} singlets from δ = 3.72/3.75 ppm in the free peptides to δ = 3.64/3.62 ppm in the bifunctional complexes. The resonances of the *trans*-sited DMF ligand (CD_3OD solution) are observed with appropriate integral values at δ = 2.84, 2.98 (CH_3) and 7.96 (CH) in **7** and 2.85, 2.97 (CH_3) and 7.96 (CH) ppm in **8**.

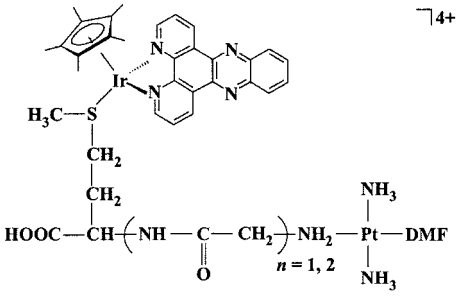

7, n = 1; **8**, n = 2

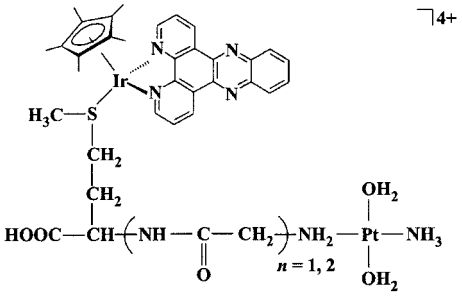

9, n = 1; **10**, n = 2

Figure 6. Tetracations of the bifunctional complexes **7**–**10**.

Bifunctional organometallic compounds of the type $[\{(\eta^5\text{-Cp*})Ir(dppz)\}(\mu\text{-peptide-}\kappa S{:}\kappa N_{G1})(trans\text{-}\{Pt(NH_3)(OH_2)_2\})][Et_4N](CF_3SO_3)_5$ **9** and **10** are prepared by reaction of the starting compounds $[(\eta^5\text{-Cp*})Ir(dppz)(peptide\text{-}\kappa S)](CF_3SO_3)_2$ with $(Et_4N)[PtCl_3(NH_3)]$ in aqueous solution following initial precipitation and removal of AgCl on treatment of the Pt^{II} complex with 3 equiv. of $Ag(CF_3SO_3)$. Although the molecular ions, themselves, could not be detected by FAB mass spectrometry, the bridging μ-1κ*S*:2κN_{Gly1} coordination mode is clearly confirmed for the peptides H-Gly-Met-OH (**9**) and H-Gly-Gly-Met-OH (**10**) by the pronounced ^{1}H NMR upfield shifts of their δ_{Met}-CH_3 and α_{Gly1}–CH_2 singlets to δ = 1.79/3.64 and 1.81/3.64 ppm, respectively. The much stronger *trans* effect of NH_3 in comparison to the aqua ligands (E_t values 200:1)[26] leads to exclusive κ*N* coordination of the peptide amino group in *trans* position to the ammine ligand in **9** and **10**. Sharp singlets for Me α_{Gly1}–CH_2 protons are also in accordance with the presence of only the *trans* isomer.

Before turning in detail to DNA interaction studies of the bifunctional complexes **7**–**10** with their complementary covalent and intercalative binding capabilities, it is necessary to consider possible competitive substitution reactions for the nucleobase nitrogen atoms, i.e. whether Ir^{III} or Pt^{II} will be preferred as coordination partners. The kinetics of nucleobase binding was, therefore, studied by ^{1}H NMR in an exemplary manner for the reaction of **7** with the model purine base 9-ethylguanine at a 1:2 molar ratio in a 10 mM phosphate buffer (pH = 7.2) at T = 298 K (Figure 7). As indicated by the rapid growth in the free DMF CH singlet at δ = 7.94 ppm in comparison to the declining resonance at δ = 7.90 ppm (coordinated DMF), substitution by the hydrogen- or dihydrogenphosphate buffer anions is relatively rapid. The extent of the subsequent slow replacement of the new anionic ligand by κ*N*7-coordinated 9-ethylguanine can be gauged by the integral ratio of the H8 resonances at δ = 8.32 (coordinated) and 7.80 (free) ppm. After 5 d, ca. 90% of **7** is converted into $[\{(\eta^5\text{-Cp*})Ir(dppz)\}(\mu\text{-H-Gly-Met-OH-}\kappa S{:}\kappa N_{G1})[trans\text{-}\{Pt(9\text{-ethylguanine})(NH_3)_2\}]]^{4+}$ (**11**) depicted in Figure 8. Exclusive Pt^{II} coordination is confirmed by the unchanged resonance positions and integral values for the dppz and δ_{Met} protons after this period of time.

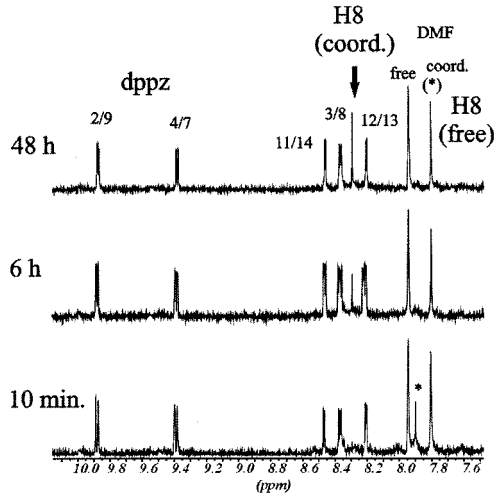

Figure 7. Aromatic region of the ^{1}H NMR spectrum of a 1:2 reaction mixture of **7** (c = 5 mM) and 9-ethylguanine in a 10 mM phosphate buffer at pH = 7.2 and T = 298 K.

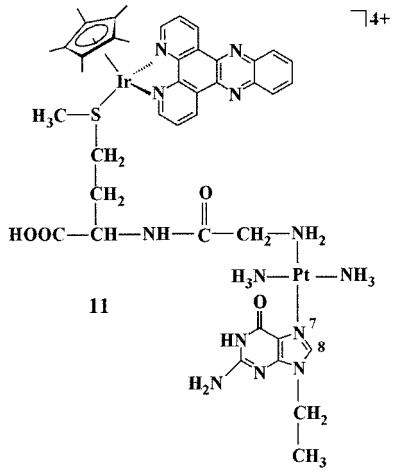

11

Figure 8. Product **11** of the reaction between **7** and 9-ethylguanine.

UV/Vis DNA Binding Studies for 7–10

The interaction of **7**–**10** with CT DNA was studied by UV/Vis titrations, DNA melting temperature determinations and CD spectroscopy. As for **3**–**6**, hypo- and bathochromic shifts were observed for the dppz absorption maxima at 363 and 382 nm on increasing the DNA/complex molar ratio from 1:1 to 15:1. Although ca. 90–95% of the total decrease in absorbance $\Delta A/A$ at 382 nm is achieved within 2 min, it takes between 8 (complex **7**) and 40 h (complex **9**) for the DNA/complex reaction mixtures to reach an equilibrium. This behaviour is in striking contrast to **3**–**6**, for which $-\Delta A/A$ reaches its maximum value within 2 min, and indicates that a slow structural reorganisation and binding optimisation must take place for **7**–**10** following rapid initial intercalation and/or surface base stacking. All UV/Vis spectra employed for the determination of binding constants and site sizes were measured after equilibration, i.e. after no further change in the monitored absorbance at 382 nm was recorded.

DNA binding parameters for **7**–**10** are listed in Table 2. As satisfactory least-squares fits (Figure 9) could be obtained in all cases for the absorption data using the model by Bard and Thorp[22,23] non-cooperative non-specific binding can be assumed for the interaction of the complexes with CT DNA. The low $-\Delta A/A$ value of 27.5% and the physically unrealistic site size (s = 0.9) of less than one base pair between binding sites indicate that only a limited degree of intercalation is achieved by **7** with its dipeptide bridging ligand H-Gly-Met-OH. A comparison of these values with those of the monofunctional complex [(η^5-Cp*)-Ir(dppz)(H-Gly-Met-OH-κ*S*)]$(CF_3SO_3)_2$[27] [$-\Delta A/A$ = 45.1%, $K_b = 1.9(7)\times10^6$ M^{-1}, s = 2.2(1)], for which equilibration is reached within 2 min, suggests that coordination of the Pt^{II} centres by DNA nucleobases must be rapid for **7**. Exclusive initial intercalation of the [(η^5-Cp*)Ir-(dppz)]$^{2+}$ fragment (as observed for the monofunctional complex), followed by a slow increase in κ*N* coordination of the group 10 metal and a concomitant reduction in the degree of intercalation, would otherwise lead to a slow decline in $\Delta A/A$ from a maximum value of ca. 45.1%[27] after 2 min.

Table 2. $-\Delta A/A$ (for λ = 382 nm), binding constants K_b, site sizes s, melting temperature shifts ΔT_m and induced circular dichroism Θ (for λ = 300 nm) for the interaction of CT DNA with complexes **7**–**10** in a 10 mM phosphate buffer at pH = 7.2.

Complex	$-\Delta A/A$ [%]	K_b [M^{-1}]	s	ΔT_m [°C]	[Θ] [deg·cm^2·dmol^{-1}]
7	27.5	$1.1(2)\times10^6$	0.9(1)	8.2	-1.5×10^3
8	35.2	$4(3)\times10^6$	2.4(2)	11.2	-2.9×10^3
9	43.9	$1.1(5)\times10^6$	1.3(1)	17.2	-3.8×10^3
10	38.5	$1.4(7)\times10^6$	2.1(1)	17.2	-3.8×10^3

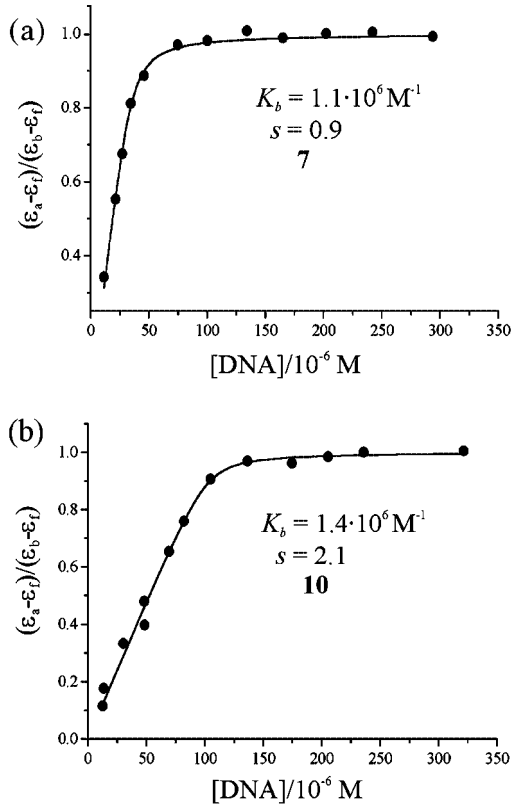

Figure 9. Best least-squares fits to the model by Bard and Thorp[22,23] for complexes **7** and **10**.

Circular Dichroism DNA Binding Studies for 7–10

In contrast to **7**, the much higher $-\Delta A/A$ and s values of 35.2% and 2.4(2), respectively, for **8** indicate that this complex with its longer bridging peptide, H-Gly-Gly-Met-OH, is apparently capable of combining both κ*N* coordination of the DNA nucleobases by the *trans*-[$Pt(NH_3)_2$(peptide-κ*N*)]$^{2+}$ fragment and effective intercalation of the [(η^5-Cp*)-Ir(dppz)(peptide-κ*S*)]$^{2+}$ moiety. Characteristic changes in the observed circular dichroism (CD) spectrum of DNA provide a means of monitoring both conformational changes for the biopolymer and possible intercalation or groove binding of an interacting metal complex.[28,29] As depicted for CT DNA in Figure 10, a negative band at

246 nm and a positive band at 275 nm due to base stacking are observed for a B-DNA helix. Addition of the metallointercalator [(η^5-Cp*)Ir(dppz)(H-Gly-Gly-Met-OH-κ*S*)](CF_3SO_3)$_2$ at a complex/DNA molar ratio of r = 0.1 leads to a small reduction in the negative Cotton effect at 246 nm and a small hypsochromic shift of 3 nm for the positive band to 272 nm, thereby indicating only minor distortion of the B helix. The additional negative-induced CD band at 300 nm must presumably be caused by the intercalation of the dppz ligands into the DNA helix.[29]

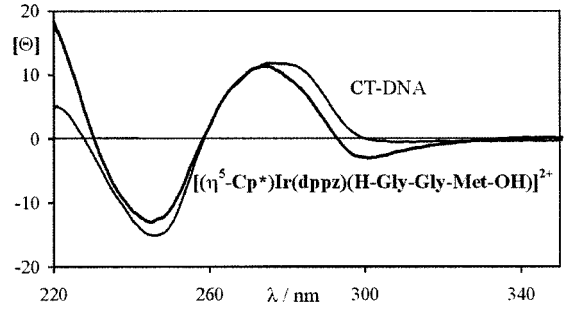

Figure 10. CD spectra of CT DNA and a mixture of [(η^5-Cp*)-Ir(dppz)(H-Gly-Gly-Met-OH-κ*S*)](CF_3SO_3)$_2$ and DNA [molar ratio (1:10)] in a 10 mM phosphate buffer (pH = 7.2) after 48 h incubation at 295 K.

Figure 11 compares the CD spectra of the bifunctional complexes **7** and **8** with CT DNA at a molar ratio of 0.1. The significantly higher degree of intercalation for **8** leads to a molar ellipticity ([Θ] = -2.9×10^3 deg·cm^2·dmol^{-1} for λ = 300 nm) that is almost twice as large as that recorded for the less effective metallointercalator **7** ([Θ] = -1.5×10^3 deg·cm^2·dmol^{-1} for λ = 300 nm). In the case of the former complex, the small but significant increase in [Θ] for the positive CD band at 276 nm may be attributed to additional

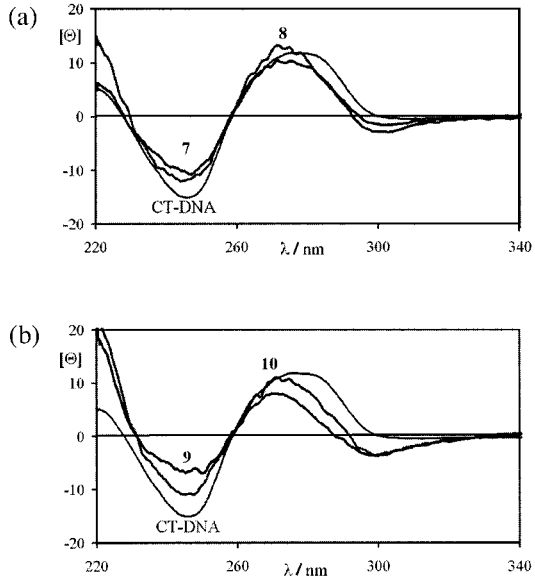

Figure 11. CD spectra of (a) complexes **7** and **8** and (b) complexes **9** and **10** with CT DNA at a complex/[DNA] molar ratio of 1:10 in a 10 mM phosphate buffer (pH = 7.2) at 295 K after 48 h incubation. [Θ] values are given in deg·cm^2·dmol^{-1}·10^3.

stabilisation of base stacking in the helix due to the combination of both dppz intercalation (see Figure 10) and covalent binding of the Pt^{II} centres. In contrast, the decrease in [Θ] for **7** at this wavelength is comparable with that previously reported for [PtCl(dien)]Cl[30] and can, therefore, be regarded as being indicative for monodentate Pt^{II} coordination with a significantly lower degree of intercalation. The large decrease in the negative [Θ] values at 246 nm in both **7** and **8** in comparison to [(η^5-Cp*)Ir(dppz)(H-Gly-Gly-Met-OH-κS)](CF_3SO_3)$_2$ (Figure 10) may be due to the fourfold positive charge of the bifunctional complexes, which could lead to a change in the helical conformation. A schematic illustration of a possible long-range simultaneous covalent and intercalative binding mode for complex **8** with s = 2.0 (calcd. 2.4) is given in Figure 12a.

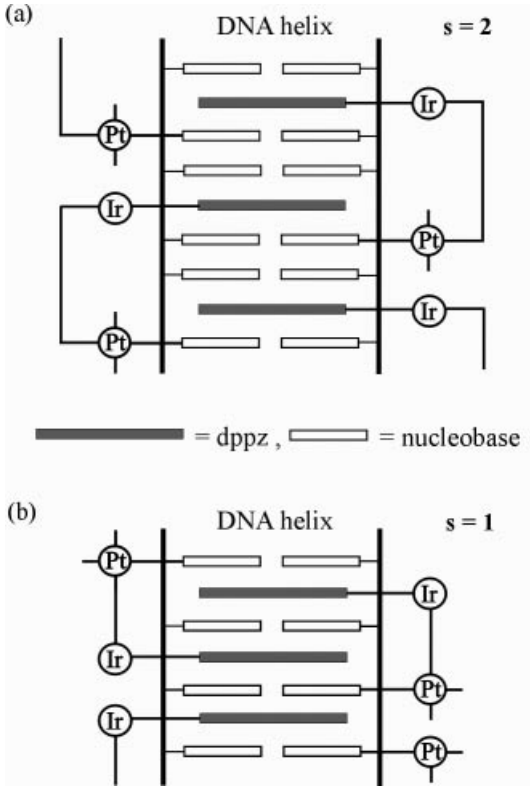

Figure 12. Schematic depictions of possible simultaneous covalent and intercalative binding modes; (a) for **8** with s = 2.0 (calcd. 2.4); (b) for **9** with s = 1.0 (calcd. 1.3).

The *cis* positions of the labile aqua ligands relative to the coordinating amino groups of the peptide ligands in **9** and **10** might be expected to favour a high degree of simultaneous covalent and intercalating DNA binding even for the shorter dipeptide of **9**. Experimental support for this hypothesis is provided by their induced molar ellipticity [Θ] at λ = 300 nm (-3.8×10^3 deg·cm^2·dmol^{-1}) and by the high values of $-\Delta A/A$ (43.9, 38.5%) and K_b (1.1×10^6, 1.4×10^6 M^{-1}) observed for their UV/Vis titrations with CT DNA at 382 nm. The former parameters are particularly interesting for **9**, as they indicate highly effective dppz intercalation for a low average site size of only 1.3 base pairs. In contrast to **10**, for which only the negative band at 247 nm is signifi-

cantly influenced by metal binding, marked decreases in the intensity are observed for both the positive and negative bands in the CD spectrum recorded for **9**/DNA at a 1:10 molar ratio. The magnitude of these decreases is similar to those observed for *trans*-$[PtCl_2(NH_3)_2]$,[30] which can disturb the DNA helix by participation in *trans*-bidentate binding. However, the characteristic bathochromic shifts of the CD band at maxima for this coordination mode are missing for both **9** and **10**. It can be concluded that **9** and **10** must both exhibit a high degree of simultaneous covalent and intercalative DNA binding and that a more pronounced reorganisation of the DNA conformation is required to achieve this goal with complex **9** with its shorter linking peptide. The high melting temperature shifts ΔT_m of 17.2 °C for the interaction mixtures **9**/DNA and **10**/DNA result presumably from increased electrostatic stabilisation of the double helix due to the presence of an additional $[Et_4N]^+$ cation. The schematic depiction of possible simultaneous covalent and intercalative binding for **9** violates the general rule of the neighbour-exclusion principle,[31] that intercalative binding can only occur at every other base pair ($s \geq 2$). Neighbour-exclusion violating structures are more rigid[32] and support for this type of structure is provided by the pronounced helix distortions evident from the CD spectra of the interaction mixture **9**/DNA (Figure 11b).

The present work, therefore, confirms that bifunctional complexes of the type $[\{(\eta^5\text{-Cp*})Ir(dppz)\}(\mu\text{-peptide-}\kappa S{:}\kappa N)\{trans\text{-}(PtL_2L')\}]^{4+}$ with flexible bridging peptide ligands are capable of simultaneous covalent and intercalative DNA binding. Both the chain length of the peptide backbone and the position of the labile ligands in the square-planar Pt^{II} coordination sphere are shown to exhibit an important influence on the degree of intercalation and the extent of helix distortion.

Experimental Section

General: All manipulations and reactions were performed under argon in carefully dried solvents using standard Schlenk techniques. FTIR: Perkin–Elmer 1760X as KBr discs. CD: Jasco J-715 in the range 220–400 nm for 1:10 complex/[DNA] mixtures [DNA concentration in M(nucleotide)] in a 10 mM phosphate buffer at pH = 7.2. FAB MS: Fisons VG Autospec with 3-nitrobenzyl alcohol as the matrix. ^1H and ^{13}C NMR spectroscopy: Bruker DRX 400 with chemical shifts reported as δ values relative to the signal of the deuterated solvent. ^{13}C NMR signals for the CF_3SO_3 anions are observed in the range δ = 121.8–122.8 (q) ppm and are not listed for individual complexes. Elemental analyses: Vario EL of Elementar Analysensysteme GmbH. $IrCl_3{\cdot}xH_2O$, K_2PtCl_4, *cis*-$[PtCl_2(NH_3)_2]$ and *trans*-$[PtCl_2(NH_3)_2]$ were purchased from Chempur, $Ag(CF_3SO_3)$ and $AgNO_3$ from Acros and peptides, with the exception of H-$(Ala)_4$-Met-OH, from Bachem. The mentioned pentapeptide was prepared by solid-state synthesis, $[\{(\eta^5\text{-Cp*})IrCl\}_2(\mu\text{-Cl})_2]$,[33] [PtCl(terpy)]Cl[34] and dipyrido[3,2-*a*:2′,3′-*c*]-phenazine (dppz)[35] in accordance with literature procedures. Subsequent treatment of an acetone solution of $[\{(\eta^5\text{-Cp*})IrCl\}_2(\mu\text{-Cl})_2]$ with 4 equiv. of $Ag(CF_3SO_3)$ and filtration of the resulting AgCl precipitate afforded the starting compound $[(\eta^5\text{-Cp*})Ir(acetone)_3](CF_3SO_3)_2$ (**1**).[17] $[(\eta^5\text{-Cp*})Ir(dppz)(H\text{-Gly-Met-OH-}\kappa S)](CF_3SO_3)_2$[16] and $[(\eta^5\text{-Cp*})Ir(dppz)(H\text{-Gly-Gly-Met-OH-}\kappa S)](CF_3SO_3)_2$ were prepared from **1** and the relevant peptide in a manner previously described for the latter complex.[14] $(Et_4N)[PtCl_3(NH_3)]$ was obtained according to a literature procedure on treating *cis*-$[PtCl_2(NH_3)_2]$ with $(Et_4N)Cl{\cdot}H_2O$.[36]

$[(\eta^5$-Cp*)Ir(dppz)(H-Gly-Gly-Phe-Met-OH-κS)$](CF_3SO_3)_2$ (3): The ligand dppz (56.5 mg, 0.2 mmol) was added to **1** (159.8 mg, 0.2 mmol) in CH_3OH/CH_2Cl_2 (10 mL) and the resulting solution stirred at reflux for 2 h. After addition of H-Gly-Gly-Phe-Met-OH (82.1 mg, 0.2 mmol) in CF_3COOH (1.5 mL) and stirring at 50 °C for 18 h, the volume was reduced to 3 mL. The product was precipitated by addition of diethyl ether, washed and dried in vacuo. Yield 181.9 mg (69%). $C_{48}H_{51}F_6IrN_8O_{11}S_3$ (1318.3): calcd. C 43.7, H 3.9, N 8.5, S 7.3; found C 43.3, H 3.8, N 8.4, S 7.3. FAB MS: *m*/*z* (%) = 1319 (17) $[M]^+$, 1168 (10) $[M - OTf]^+$, 1019 (44) $[M - 2\ OTf]^+$. ^1H NMR (CD_3OD): δ = 1.79 (s, 3 H, δ Met), 1.84 (s, 15 H, CH_3 Cp*), 1.9–2.1 (mm, 4 H, β and γ Met), 2.93, 3.14 (m, 2 H, β Phe), 3.65, 3.69 (2s, 4 H, α Gly1, α Gly2), 4.29 (m, 1 H, α Phe), 4.36 (m, 1 H, α Met), 7.15 (m, 4 H, Phe), 7.24 (s, 1 H, Phe), 8.11 (m, 2 H), 8.43 (m, 2 H), 8.49 (dd, 2 H), 9.37 (dd, 2 H), 10.04 (dd, 2 H, dppz) ppm. ^{13}C NMR (CD_3OD): δ = 8.6 (CH_3 Cp*), 17.0 (δ Met), 30.6 (β Met), 33.7 (γ Met), 38.2 (β Phe), 41.6, 43.4 (α Gly), 51.0 (α Met), 56.2 (α Phe), 97.2 (Cp*), 127.8, 129.6, 130.3 (Phe), 130.4, 130.9 (dppz), 131.0 (Phe), 133.8, 134.3, 139.2, 140.6, 144.3, 151.3, 155.2 (dppz), 168.1, 171.1, 172.7, 173.6 (COO, NHCO) ppm. IR: $\tilde{\nu}$ = 3436 vs. (NH), 1737, 1675 s (ν CO), 1545, 1499 (δ NH) cm^{-1}.

$[(\eta^5$-Cp*)Ir(dppz)[H-$(Ala)_4$-Met-OH-κS]$](CF_3SO_3)_2$ (4): Preparation as for **3** with H-$(Ala)_4$-Met-OH (86.7 mg, 0.2 mmol). Yield 139.5 mg (52%). $C_{47}H_{56}F_6IrN_9O_{12}S_3$ (1341.4): calcd. C 42.1, H 4.2, N 9.4, S 7.2 (%); found C 42.3, H 3.8, N 9.1, S 6.7 (%). FAB MS: *m*/*z* (%) = 1341 (12) $[M]^+$, 1192 (11) $[M - OTf]^+$, 1042 (10) $[M - 2\ OTf]^+$. ^1H NMR (CD_3OD): δ = 1.33 (mm, 9 H, β Ala), 1.49 (m, 3 H, β Ala), 1.79 (s, 3 H, δ Met), 1.84 (s, 15 H, CH_3 Cp*), 1.9–2.1 (mm, 4 H, β and γ Met), 3.94, 4.10, 4.21 (3m, 3 H, α Ala), 4.35 (m, 2 H, α Ala und α Met), 8.17 (dd, 2 H), 8.44 (m, 2 H), 8.54 (dd, 2 H), 9.39 (m, 2 H), 10.05 (dd, 2 H, dppz) ppm. ^{13}C NMR (CD_3OD): δ = 9.1 (CH_3 Cp*), 17.3 (δ Met), 17.9, 18.1, 18.3, 18.4 (β Ala), 31.4 (β Met), 34.5 (γ Met), 50.4, 50.7, 50.9 (α Ala), 52.6 (α Met), 97.4 (Cp*), 130.8, 131.2, 133.0, 134.3, 138.5, 141.0, 144.6, 151.7, 155.4 (dppz), 167.1, 171.1, 174.9, 175.4, 182.1 (COO, NHCO) ppm. IR: $\tilde{\nu}$ = 3435 s (NH), 1664 (ν CO), 1543, 1499 (δ NH) cm^{-1}.

$[\{(\eta^5$-Cp*)Ir(dppz)$\}(\mu$-H-Gly-Gly-Phe-Met-OH-κS:κN$)\{$Pt-(terpy)$\}](CF_3SO_3)_4$ (5): $Ag(CF_3SO_3)$ (102.8 mg, 0.4 mmol) was added to [PtCl(terpy)]Cl·$2H_2O$ (107.1 mg, 0.2 mmol) in H_2O (10 mL) and stirred in the dark for 24 h. After removal of precipitated AgCl and addition of **3** (263.7 mg, 0.2 mmol), the clear solution was stirred at 50 °C for 18 h. The solvent was removed and the resulting solid redissolved in CH_3OH (3 mL). Following precipitation with diethyl ether, the product was washed and dried in vacuo. Yield 171.8 (42%). $C_{65}H_{62}F_{12}IrN_{11}O_{17}PtS_5$ (2044.9): calcd. C 38.2, H 3.1, N 7.5, S 7.8; found C 38.8, H 3.4, N 7.0, S 7.8. FAB MS: *m*/*z* (%) = 1895 (5) $[M - OTf]^+$, 1319 (13) $[M - 2\ OTf - Pt(terpy)]^+$, 1019 (12) $[M - 4\ OTf - Pt(terpy)]^+$. ^1H NMR (CD_3OD): δ = 1.81 (s, 3 H, δ Met), 1.84 (s, 15 H, CH_3 Cp*), 1.9–2.1 (mm, 4 H, β and γ Met), 3.61, 3.68 (2s, 4 H, α Gly1, α Gly2), 4.32 (m, 1 H, α Phe), 4.39 (m, 1 H, α Met), 7.15 (mm, 5 H, Phe), 7.82 (m, 2 H, terpy H5), 8.11 (m, 2 H, dppz), 8.3–8.5 (mm, 11 H, terpy and dppz), 8.83 (m, 2 H, terpy H6), 9.37 (m, 2 H), 10.03 (dd, 2 H, dppz) ppm. ^{13}C NMR (CD_3OD): δ = 8.5 (CH_3 Cp*), 17.0 (δ Met), 30.5 (β Met), 33.8 (γ Met), 37.1 (β Phe), 41.6, 43.5 (α Gly), 52.5 (α Met), 56.4 (α Phe), 97.2 (Cp*), 125.4, 126.7 (terpy), 127.8,

129.5, 130.2 (Phe), 130.4, 131.0, 133.8, 134.0, 139.2, 141.0 (dppz), 144.0, 144.2 (terpy), 144.5 (dppz), 148.8 (terpy), 151.6, 155.6 (dppz), 168.3, 170.9 (COO, NHCO) ppm. IR: $\tilde{\nu}$ = 3448 s (NH), 1664 (ν CO), 1543 (δ NH) cm^{-1}.

[{(η⁵-Cp*)Ir(dppz)}(μ-H-(Ala)₄-Met-OH-κ*S*:κ*N*$_{A1}$){Pt(terpy)}](CF₃SO₃)₄ (6): Preparation as for **5** with **4** (268.3 mg, 0.2 mmol). Yield 140.6 mg (34%). $C_{64}H_{67}F_{12}IrN_{12}O_{18}PtS_5$ (2067.9): calcd. C 37.2, H 3.3, N 7.8, S 8.1; found C 37.1, H 3.1, N 8.1, S 8.0. FAB MS: *m*/*z* (%) = 1919 (1) $[M - OTf]^+$, 1042 (17) $[M - 4\ OTf - Pt(terpy)]^+$. ^1H NMR (CD_3OD): δ = 1.32 (mm, 9 H, β Ala), 1.49 (d, 3 H, β Ala), 1.79 (s, 3 H, δ Met), 1.84 (s, 15 H, CH_3 Cp*), 1.9–2.1 (mm, 4 H, β and γ Met), 3.72, 4.10, 4.21 (3m, 3 H, α Ala), 4.35 (m, 2 H, α Ala und α Met), 7.82 (m, 2 H, terpy H5), 8.16 (dd, 2 H, dppz), 8.3–8.6 (mm, 11 H, terpy and dppz), 8.88 (m, 2 H, terpy H6), 9.37 (m, 2 H), 10.05 (dd, 2 H, dppz) ppm. ^{13}C NMR (CD_3OD): δ = 8.5 (CH_3 Cp*), 16.7 (δ Met), 17.6, 17.8, 18.1 (β Ala), 31.4 (β Met), 33.9 (γ Met), 50.2, 50.6, 50.7, 50.8 (α Ala), 51.8 (α Met), 97.2 (Cp*), 123.4, 125.4 (terpy), 130.7, 131.0, 133.6, 134.0, 139.1, 140.5, 144.5 (dppz), 148.7 (terpy), 151.5 (dppz), 151.7 (terpy), 155.7 (dppz), 156.9, 159.1 (terpy), 170.9, 174.5, 175.1 (COO, NHCO) ppm. IR: $\tilde{\nu}$ 3434 vs. (NH), 1742, 1631 (ν CO), 1528 (δ NH) cm^{-1}.

[{(η⁵-Cp*)Ir(dppz)}(μ-H-Gly-Met-OH-κ*S*:κ*N*$_{G1}$)(*trans*-{Pt(NH₃)₂(DMF)})](CF₃SO₃)₂(NO₃)₂ (7): $AgNO_3$ (68.0 mg, 0.4 mmol) was added to *trans*-$[PtCl_2(NH_3)_2]$ (60.0 mg, 0.2 mmol) in DMF (10 mL) and stirred in the dark for 24 h. After removal of precipitated AgCl and addition of [(η⁵-Cp*)Ir(dppz)(H-Gly-Met-OH-κ*S*)]$(CF_3SO_3)_2$ (222.8 mg, 0.2 mmol), the clear solution was stirred at room temperature for 18 h. The solvent was removed and the resulting solid redissolved in CH_3OH (3 mL). Following precipitation with diethyl ether, the product was washed and dried in vacuo. Yield 135.6 mg (44%). $C_{40}H_{52}F_6IrN_{11}O_{16}PtS_3$ (1540.4): calcd. C 31.2, H 3.4, N 10.0, S 6.2; found C 31.3, H 3.3, N 9.8, S 6.3. FAB MS: *m*/*z* (%) = 1043 (41) $[M - 2\ OTf - 2\ NO_3 - DMF]^+$, 1025 (12) $[M - 2\ OTf - 2\ NO_3 - DMF - NH_3]^+$. ^1H NMR (CD_3OD): δ = 1.79 (s, 3 H, δ Met), 1.82 (s, 15 H, CH_3 Cp*), 1.97 (m, 2 H, β Met), 2.16 (m, 2 H, γ Met), 2.84, 2.98 (2s, 6 H, CH_3 DMF), 3.64 (s, 2 H, α Gly), 4.40 (m, 1 H, α Met), 7.96 (s, 1 H, CH DMF), 8.16 (dd, 2 H), 8.45 (m, 2 H), 8.52 (dd, 2 H), 9.39 (m, 2 H), 10.06 (m, 2 H, dppz) ppm. ^{13}C NMR (CD_3OD): δ = 9.1 (CH_3 Cp*), 17.1 (δ Met), 31.0 (β Met), 35.1 (γ Met), 37.4 (CH_3 DMF), 41.4 (α Gly), 52.5 (α Met), 97.6 (Cp*), 130.9, 131.3, 133.4, 134.1, 138.7, 141.1, 144.7, 155.2 (dppz), 168.4, 171.5 (COO, NHCO) ppm. IR: $\tilde{\nu}$ = 3446 vs. (NH), 1684 s (ν CO), 1636 (ν CO DMF), 1496 (δ NH) cm^{-1}.

[{(η⁵-Cp*)Ir(dppz)}(μ-H-Gly-Gly-Met-OH-κ*S*:κ*N*$_{G1}$)(*trans*-{Pt(NH₃)₂(DMF)})](CF₃SO₃)₂(NO₃)₂ (8): Preparation as for **7** with [(η⁵-Cp*)Ir(dppz)(H-Gly-Gly-Met-OH-κ*S*)]$(CF_3SO_3)_2$ (234.2 mg, 0.2 mmol). Yield 147.0 mg (46%). $C_{42}H_{55}F_6IrN_{12}O_{17}PtS_3$ (1597.4): calcd. C 33.8, H 3.5, N 10.5, S 6.0; found C 33.5, H 3.7, N 10.0, S 5.8. FAB MS: *m*/*z* (%) = 1172 (14) $[M - 2\ NO_3 - DMF - Pt(NH_3)_2]^+$, 1022 (6) $[M - OTf - 2\ NO_3 - DMF - Pt(NH_3)_2]^+$. ^1H NMR (CD_3OD): δ = 1.79 (s, 3 H, δ Met), 1.84 (s, 15 H, CH_3 Cp*), 1.9–2.1 (mm, 4 H, β and γ Met), 2.85, 2.97 (2s, 6 H, CH_3 DMF), 3.62 (s, 2 H, α Gly1), 3.88 (s, 2 H, α Gly2), 4.40 (br., 1 H, α Met), 7.96 (s, 1 H, CH DMF), 8.18 (dd, 2 H), 8.45 (m, 2 H), 8.53 (dd, 2 H), 9.37 (dd, 2 H), 10.06 (dd, 2 H, dppz) ppm. ^{13}C NMR (CD_3OD): δ = 9.1 (CH_3 Cp*), 17.6 (δ Met), 30.8 (β Met), 31.9 (CH_3 DMF), 35.6 (γ Met), 37.2 (CH_3 DMF), 41.8, 43.6 (α Gly), 53.4 (α Met), 97.3 (Cp*), 130.7, 131.1, 133.8, 134.1, 139.5, 140.9, 144.6, 151.8, 155.0 (dppz), 165.1 (CH DMF), 171.7, 172.8 (COO, NHCO) ppm. IR: $\tilde{\nu}$ = 3446 vs. (NH), 1636 (ν CO DMF), 1543 (δ NH) cm^{-1}.

[{(η⁵-Cp*)Ir(dppz)}(μ-H-Gly-Met-OH-κ*S*:κ*N*$_{G1}$)(*trans*-{Pt(NH₃)(OH₂)₂})][Et₄N](CF₃SO₃)₅ (9): Preparation as for **7** with $Ag(CF_3SO_3)$ (154.2 mg, 0.6 mmol) and $(Et_4N)[PtCl_3(NH_3)]$ (89.7 mg, 0.2 mmol) in H_2O (10 mL) as starting compounds. Yield 151.3 mg (39%). $C_{48}H_{66}F_{15}IrN_8O_{20}PtS_6$ (1939.7): calcd. C 29.7, H 3.4, N 5.8, S 9.9; found C 29.5, H 2.9, N 5.5, S 9.0. FAB MS: *m*/*z* (%) = 1115 (35) $[M - 3\ OTf - Et_4N - Pt(NH_3)(OH_2)_2]^+$. ^1H NMR (CD_3OD): δ = 1.29 (tt, 12 H, CH_3 Et_4N), 1.79 (s, 3 H, δ Met), 1.84 (s, 15 H, CH_3 Cp*), 1.98 (m, 2 H, β Met), 2.15 (m, 2 H, γ Met), 3.64 (s, 2 H, α Gly), 4.40 (m, 1 H, α Met), 8.18 (dd, 2 H), 8.46 (m, 2 H), 8.54 (dd, 2 H), 9.39 (dd, 2 H), 10.07 (dd, 2 H, dppz) ppm. ^{13}C NMR (CD_3OD): δ = 7.8 (CH_3 Et_4N), 8.7 (CH_3 Cp*), 16.9 (δ Met), 30.3 (β Met), 34.4 (γ Met), 41.8 (α Gly), 52.4 (α Met), 53.5 (CH_2 Et_4N), 97.5 (Cp*), 130.8, 131.2, 133.8, 134.3, 139.4, 141.0, 144.7, 151.8, 155.8 (dppz), 174.3 (COO) ppm. IR: $\tilde{\nu}$ = 3436 vs. (NH), 1629 (ν CO), 1546 (δ NH) cm^{-1}.

[{(η⁵-Cp*)Ir(dppz)}(μ-H-Gly-Gly-Met-OH-κ*S*:κ*N*$_{G1}$)(*trans*-{Pt(NH₃)(OH₂)₂})][Et₄N](CF₃SO₃)₅ (10): Preparation as for **9** with [(η⁵-Cp*)Ir(dppz)(H-Gly-Gly-Met-OH-κ*S*)]$(CF_3SO_3)_2$ (234.2 mg, 0.2 mmol). Yield 171.7 mg (43%). $C_{50}H_{69}F_{15}IrN_9O_{21}PtS_6$ (1996.8): calcd. C 30.1, H 3.5, N 6.3, S 9.6; found C 30.1, H 3.6, N 6.6, S 9.1. FAB MS: *m*/*z* (%) = 1172 (15) $[M - 3\ OTf - Et_4N - Pt(NH_3)(OH_2)_2]^+$, 1022 (29) $[M - 4\ OTf - Et_4N - Pt(NH_3)(OH_2)_2]^+$. ^1H NMR (CD_3OD): δ = 1.29 (tt, 12 H, CH_3 Et_4N), 1.81 (s, 3 H, δ Met), 1.85 (s, 15 H, CH_3 Cp*), 1.9–2.1 (mm, 4 H, β and γ Met), 3.64 (s, 2 H, α Gly1), 3.90 (s, 2 H, α Gly2), 4.39 (br., 1 H, α Met), 8.18 (dd, 2 H), 8.47 (m, 2 H), 8.53 (dd, 2 H), 9.38 (dd, 2 H), 10.06 (dd, 2 H, dppz) ppm. ^{13}C NMR (CD_3OD): δ = 7.9 (CH_3 Et_4N), 8.8 (CH_3 Cp*), 17.2 (δ Met), 30.1 (β Met), 34.1 (γ Met), 41.9, 43.6 (α Gly), 52.1 (α Met), 53.6 (CH_2 Et_4N), 97.5 (Cp*), 130.9, 131.3, 133.9, 134.4, 139.5, 141.2, 144.8, 151.8, 155.8 (dppz), 168.4, 171.7 (COO, NHCO) ppm. IR: $\tilde{\nu}$ = 3436 vs. (NH), 1629 (ν CO), 1499 (δ NH) cm^{-1}.

DNA Binding Studies of 3–10: The thermal denaturation temperature T_m of 1:10 complex/DNA mixtures was determined in a 10 mM phosphate buffer at pH = 7.2. Melting curves were recorded at 260 nm with a Lambda 15 Perkin–Elmer spectrometer connected with a temperature controller (Haake FS thermostat). A ramp rate of 0.25 °C min^{-1} was used over the range 25–97 °C. T_m values were calculated by determining the midpoints of the melting curves from the first-order derivatives. Experimental ΔT_m values are estimated to be accurate within ±1. Concentrations of CT DNA were determined spectrophotometrically using the molar extinction coefficient ε_{260} = 6600 M^{-1} cm^{-1}.[37] All absorption titrations were performed at room temperature. After sonication, buffered solutions of CT DNA gave a ratio of UV absorbance A_{260}/A_{280} of ca. 1.90, indicating that DNA was sufficiently free of protein.[38] 20 μM solutions of the individual metal complexes were treated with DNA over a range of molarities from 20 to 400 μM (nucleotide). All UV/Vis spectra were measured after equilibration, i.e. no further change in monitored absorbance. Titration curves were constructed from the fractional change in the absorbance as a function of DNA concentration according to the model by Bard and Thorp[22,23] for non-cooperative non-specific binding for one type of discrete DNA binding site.

$$(\varepsilon_a - \varepsilon_f)/(\varepsilon_b - \varepsilon_f) = (b - \{b^2 - 2K_b{}^2C_t[\mathrm{DNA}]/s\}^{1/2})/2K_bC_t \quad (1)$$

Equation (1) was used to fit the absorption data by least-squares refinement of binding constants (K_b) and site sizes (s) with $b = 1 + K_bC_t + K_b[\mathrm{DNA}]/2s$, where ε_a is the extinction coefficient observed at a given DNA concentration, ε_f the extinction coefficient of the complex in the absence of DNA, ε_b the extinction coefficient

of the complex when fully bound to DNA (i.e. no absorption change on further addition of DNA), K_b the equilibrium constant in M^{-1}, C_t the total metal complex concentration, [DNA] the DNA concentration in M(nucleotide), and s the binding site size. Values of ε_b were obtained by extrapolation from the y intercept of plots of $\varepsilon_a/\varepsilon_f$ vs. 1/[DNA]. The K_b and s values of Tables 1 and 2 are those for the best least-squares fits to the individual UV/Vis titration curves using the program ORIGIN 6.0.

X-ray Structural Analysis of 2: $[(\eta^5\text{-Cp*})Ir(CF_3COO)(dppz)](CF_3SO_3)$, $C_{31}H_{25}F_6IrN_4O_5S$, M = 871.8, triclinic, space group $P\bar{1}$ (no. 2), a = 8.701(2), b = 11.535(2), c = 16.603(3) Å, α = 103.60(3), β = 90.93(3), γ = 102.21(3)°, V = 1579.2(5) Å^3, Z = 2, $D_{calcd.}$ = 1.833 g·cm^{-3}, μ(Mo-K_α) = 4.376 mm^{-1}; Siemens P4 diffractometer; graphite-monochromated Mo-K_α radiation (λ = 0.71073 Å). Crystal size: 0.46 × 0.30 × 0.12 mm; ω-scan in the range $2\theta \leq 50°$ ($-10 \leq h \leq 10$, $0 \leq k \leq 13$, $-19 \leq l \leq 19$), 5683 reflections collected, 5406 independent reflections (R_{int} = 0.051); semiempirical absorption corrections with ψ-scans; max./min. transmission 0.716/0.373; 428 parameters refined; R_1 = 0.057 for 4326 reflections with $I > 2\sigma(I)$, $wR_2 = \{[\Sigma w(F_o^2 - F_c^2)^2]/[\Sigma w(F_o)^2]\}^{1/2}$ = 0.136 for all data; min./max. residual electron density 1.82/–1.83 e·Å^{-3}. Anisotropic temperature factors for all non-hydrogen atoms with the exception of the disordered F atoms of the CF_3COO^- ligand, which exhibit s.o.f. values of 0.8 and 0.2.[39]

[1] N. Farrell, Y. Qu, U. Bierbach, M. Valsecchi, E. Mertz, in: *Cisplatin: Chemistry and Biochemistry of a Leading Anticancer Drug* (Ed.: B. Lippert), Wiley-VCH, Weinheim, **1999**, pp. 479–496.

[2] N. Farrell, in: *Platinum-Based Drugs in Cancer Therapy* (Eds.: L. R. Kelland, N. Farrell), Humana Press, Totowa, **2000**, pp: 321–338.

[3] N. J. Wheate, J. G. Collins, *Coord. Chem. Rev.* **2003**, *241*, 133–145.

[4] Y. Qu, N. Farrell, *Inorg. Chem.* **1995**, *34*, 3573–3576.

[5] K. van der Schilden, F. Garcia, H. Kooijman, A. L. Spek, J. G. Haasnoot, J. Reedijk, *Angew. Chem. Int. Ed.* **2004**, *43*, 5786–5788.

[6] B. E. Bowler, K. J. Ahmed, W. I. Sundquist, L. S. Hollis, E. E. Whang, S. J. Lippard, *J. Am. Chem. Soc.* **1989**, *111*, 1299–1306.

[7] M. D. Temple, W. D. McFadyen, R. J. Holmes, W. A. Denny, V. Murray, *Biochemistry* **2000**, *39*, 5593–5599.

[8] L. C. Perrin, C. Cullinane, W. D. McFadyen, D. R. Phillips, *Anti-Cancer Drug Des.* **1999**, *14*, 243–252.

[9] L. C. Perrin, P. D. Prenzler, C. Cullinane, D. R. Phillips, W. A. Denny, W. D. McFadyen, *J. Inorg. Biochem.* **2000**, *81*, 111–117.

[10] W. D. McFadyen, L. P. G. Wakelin, I. A. G. Roos, B. L. Hillcoat, *Biochem. J.* **1986**, *238*, 757–763.

[11] H. Kurosaki, N. Yamakawa, M. Sumimoto, K. Kimura, M. Goto, *Bioorg. Med. Chem. Lett.* **2003**, *13*, 825–828.

[12] B. Önfelt, P. Lincoln, B. Norden, *J. Am. Chem. Soc.* **1999**, *121*, 10846–10847.

[13] K. E. Erkkila, D. T. Odom, J. K. Barton, *Chem. Rev.* **1999**, *99*, 2777–2795.

[14] D. Herebian, W. S. Sheldrick, *J. Chem. Soc. Dalton Trans.* **2002**, 966–974.

[15] A. Frodl, D. Herebian, W. S. Sheldrick, *J. Chem. Soc. Dalton Trans.* **2002**, 3664–3673.

[16] R. Stodt, S. Gençaslan, A. Frodl, C. Schmidt, W. S. Sheldrick, *Inorg. Chim. Acta* **2003**, *355*, 242–253.

[17] C. White, S. J. Thompson, P. M. Maitlis, *J. Organomet. Chem.* **1977**, *127*, 415–421.

[18] G. Schwarz, S. Klose, W. Balthasar, *Eur. J. Biochem.* **1970**, *12*, 454–460.

[19] K. W. Jennette, J. T. Gill, J. A. Sadownick, S. J. Lippard, *J. Am. Chem. Soc.* **1976**, *98*, 6159–6168.

[20] W. S. Sheldrick, S. Heeb, *J. Organomet. Chem.* **1989**, *377*, 357–366.

[21] W. S. Sheldrick, A. Gleichmann, *J. Organomet. Chem.* **1994**, *470*, 183–187.

[22] M. T. Carter, M. Rodriguez, A. J. Bard, *J. Am. Chem. Soc.* **1989**, *111*, 8901–8911.

[23] S. R. Smith, G. A. Neyhart, W. A. Karlsbeck, H. H. Thorp, *New J. Chem.* **1994**, *18*, 397–406.

[24] M. Hahn, M. Kleine, W. S. Sheldrick, *J. Biol. Inorg. Chem.* **2001**, *6*, 556–566.

[25] M. Kleine, D. Wolters, W. S. Sheldrick, *J. Inorg. Biochem.* **2003**, *97*, 354–363.

[26] L. I. Elding, O. Gröning, *Inorg. Chem.* **1978**, *7*, 1872–1880.

[27] S. Gençaslan, *Dissertation*, Ruhr-Universität Bochum, **2004**.

[28] V. Brabec, V. Kleinwächter, J.-L. Butour, N. P. Johnson, *Biophys. Chem.* **1990**, *35*, 129–141.

[29] D. M. Gray, in: *Circular Dichroism and the Conformational Analysis of Biomolecules* (Ed.: G. D. Fasman), Plenum Press, New York, **1996**, pp. 469–500.

[30] J.-P. Macquet, J.-L. Butour, *Eur. J. Biochem.* **1978**, *83*, 375–387.

[31] D. M. Crothers, *Biopolymers* **1968**, *6*, 575–584.

[32] S. N. Rao, P. A. Kollman, *Proc. Nat. Acad. Sci. USA* **1987**, *84*, 5735–5739.

[33] a) J. W. Kang, K. Moseley, P. M. Maitlis, *J. Am. Chem. Soc.* **1969**, *91*, 5970–5977; b) B. L. Booth, R. N. Haszeldine, M. Hill, *J. Chem. Soc. A* **1969**, 1299–1303.

[34] G. Annibale, M. Brandolisio, B. Pitteri, *Polyhedron* **1995**, *3*, 451–453.

[35] M. Yamada, Y. Tanaka, Y. Yoshimoto, *Bull. Chem. Soc. Jpn.* **1992**, *65*, 1006–1011.

[36] M. J. Abrams, C. M. Giandomenico, J. F. Vollano, D. A. Schwartz, *Inorg. Chim. Acta* **1987**, *131*, 3–4.

[37] H.-Q. Liu, T.-C. Cheung, S.-M. Peng, C.-M. Che, *J. Chem. Soc. Chem. Commun.* **1995**, *17*, 1787–1788.

[38] J. Marmur, *J. Mol. Biol.* **1961**, *3*, 208–218.

[39] CCDC-266154 (**2**) contains the supplementary crystallographic data for this paper. These data can be obtained free of charge from The Cambridge Crystallographic Data Centre via www.ccdc.cam.ac.uk/data_request/cif.

Received: March 16, 2005
Published Online: August 4, 2005

